Thermodynamic uncertainty relations in mesoscopic devices

I. R. A. C. Lucena, R. A. Batista, and J. G. G. S. Ramos
Departamento de Física, Universidade Federal da Paraíba, 58051-970 João Pessoa, Paraíba, Brazil

(Received 21 October 2022; accepted 15 May 2023; published 2 June 2023)

We investigate the thermodynamic uncertainty relations (TURs) in mesoscopic devices for all universal symmetry classes of Wigner-Dyson and Dirac (chiral). The observables of interest include the TUR (MS), which is defined in terms of the ratio between the mean noise and mean conductance, as well as a new TUR (R) proposed in this article, which is based on the ensemble mean of the noise-to-conductance ratio. A detailed study is made on the quantum interference corrections associated with the TURs. We also analyze the influence of orbital and sublattice/chiral degrees of freedom for the validity of the observables in these chaotic mesoscopic billiards. Our investigation is based on the concatenation between the Landauer-Büttiker theory, the Mahaux-Wendeinmüller theory, and the TURs. We simulate the universal mesoscopic chaotic quantum dots using the random-matrix theory and compare our numerical results with the pertinent experimental data. The results were obtained for a different number of channels and tunneling rates that vary from the opaque to the ideal regime and, in all cases, demonstrate a clear phenomenological distinction between the TURs. In particular, the opaque regime engenders remarkable differences between the observables, even in the semiclassical regime, which characterizes a clear violation of the central limit theorem. Furthermore, we show that the phenomenology of the quantum interference corrections is strikingly robust, surprisingly exhibiting an order of magnitude greater than the supposedly leading semiclassical term for the TUR (R).

DOI: 10.1103/PhysRevE.107.064104

I. INTRODUCTION

Thermodynamic uncertainty relations (TURs) express a tradeoff between the accuracy of measurement (noise) and the associated entropy production rate (cost of measurement) [1–4]. On the other hand, recent technological developments have led to the creation of artificial atoms (quantum dots) whose phenomenology allows testing nonequilibrium thermodynamics and quantum mechanics at their limits [5–11]. Moreover, these nanostructured devices generate quantum stochastic transport processes, from which we identify manifestations of quantum interference [12–15], universal fluctuations [16], thermal noise, quantum noise [17–21], and other significant contributions not expected in the corresponding classical electronic current.

Over the last decade, many formalisms have been used to provide general [22–24] and unified TURs, such as Ref. [25], that derives and generalizes uncertainty relations from fluctuation theorems (FTs) [26–28]. A natural question that emerges is about the magnitude of these thermodynamic corrections when compared to the quantum ones, resulting from the signatures of universal fluctuations and quantum interference, which, typically can produce localization.

The localization phenomena in the context of thermodynamics surpass fundamental aspects and find possible current technological applications. In this regard, Ref. [29] investigates localization related to isolated interacting quantum systems and demonstrates the existence of many-body localization resisting for long intervals. In particular, its analysis confirms the existence of resonant level statistics in thermalizing systems obeying the universal Gaussian orthogonal ensemble (GOE) [30], with essential applications in the context of heat engines. Usually the transport properties of mesoscopic systems are universal and dictated only by fundamental symmetries, i.e., these properties are independent of the material of which the device is composed and its specific geometry [31,32]. Initially addressed in nuclear physics and improved on mesoscopic systems, the random-matrix theory (RMT) is a powerful technique to connect underlying symmetries with the spectrum of a chaotic mesoscopic system. Physical properties such as quantum interference corrections of both conductance and shot-noise power depend, for instance, on time-reversal and spin-rotation symmetries [33,34].

Recent experiments on nanostructured electronic conductors have been carried out to study gold atomic-scale junctions [35]. Although current transport in junctions is experimentally explored in the literature, these systems offer a scattering process with one or few resonances, making the local spectrum statistics dependent on microscopic details such as the number of atoms in the junction or the position of these atoms. In this work we are interested in mesoscopic devices, also called ballistic chaotic quantum dots. On the one hand, these devices are sufficiently small that electrons maintain their quantum-mechanical phase coherence, so a classical description of the transport properties is inadequate. On the other hand, they are sufficiently large that a statistical description is meaningful. Given that, to treat this type of system we invoke the universality hypothesis of RMT, for which the local spectral statistics of a chaotic system depend only on the symmetry properties of the Hamiltonian and not on microscopic details.

For universal mesoscopic systems, a fundamental question remains in the literature about the role of quantum interference mechanisms underlying electronic transport in the TURs corrections: Are quantum symmetry mechanisms predominant

in heat engines, or does some entropy production tradeoff between process precision and dissipation have a more crucial role in FTs? For quantum systems, proposals have emerged intending to analyze nonlinear contributions on the conductance G and the shot-noise power $\mathcal{P}$ measurements [36]. In particular, for chaotic ballistic quantum dots, conductance and shot-noise power present quantum interference corrections due to the high-order scattering processes inside the cavity [37]. Therefore, as it is well known that RMT provides a framework that determines the intrinsic properties of the system, and the TURs can be defined in terms of the ratio between the time averages of the shot-noise power and the conductance, the TURs are ambiguous by this approach in the ensemble (universal) average. In this way we propose a measure called the TUR ratio (TUR-R) as an intrinsic property of the system. More clearly, the TUR-R, $Q_{\text{TUR-R}}$, is an ensemble average $[\dots]$,

$$Q_{\text{TUR-R}} = \frac{V}{k_B T}\left[\frac{\langle \mathcal{P}\rangle}{\langle G\rangle}\right], \tag{1}$$

where T is the reservoir's temperature, V is the voltage, and $\langle\dots\rangle$ is the time average taken over a single mesoscopic sample. One expects in the semiclassical regime that

$$\frac{V}{k_B T}\left[\frac{\langle \mathcal{P}\rangle}{\langle G\rangle}\right] \approx \frac{V}{k_B T}\frac{[\langle \mathcal{P}\rangle]}{[\langle G\rangle]}, \tag{2}$$

due to the law of large numbers and the central limit theorem. We also introduce the TUR-MS (TUR measuring the ratio between the noise and conductance ensemble averages separately) as

$$Q_{\text{TUR}-\text{MS}} = \frac{V}{k_B T}\frac{[\langle \mathcal{P}\rangle]}{[\langle G\rangle]}. \tag{3}$$

The TUR ratio (TUR-R) factor $Q_{\text{TUR}-\text{R}}$ proved to be revealing and valuable; that is, $Q_{\text{TUR}-\text{R}}$ provides additional information beyond the separate measurements of the electronic current and its corresponding temporal fluctuations amplitudes. When comparing such measurements involving tunneling junctions with ballistic chaotic quantum dots (CQDs), we show that quantum interference corrections in chaotic cavities are more dominant than in tunneling junctions due to the number of resonant states in the chaotic cavity. The shot noise, an intrinsically quantum part of the fluctuations of a nonequilibrium electronic current, is associated with the fact that different parts of the electron wave can go to different places. Thus the shot noise is enhanced in mesoscopic devices and, consequently, the TUR. More questions emerge from this fact: do the TUR-R and the TUR-MS undergo quantum corrections that distinguish them even more in the universal regime?

In this study we provided an answer to all these questions. To this end, we divided the paper into sections. In Sec. II we do a pedagogical review of the Landauer-Büttiker formalism, and we will build a connection with the RMT and uncertainty relations, offering a framework for the study of TUR-R and TUR-MS in the universal quantum transport regime. In Sec. III we implement the Mahaux-Weidenmüller Hamiltonian theory using the Monte Carlo method and obtain universal results for the Wigner-Dyson classes, that is, for nonrelativistic chaotic conductors described by the Schrödinger equation. We will extend the results to encompass relativistic systems [38] such as graphene and topological insulators in the universal regime.

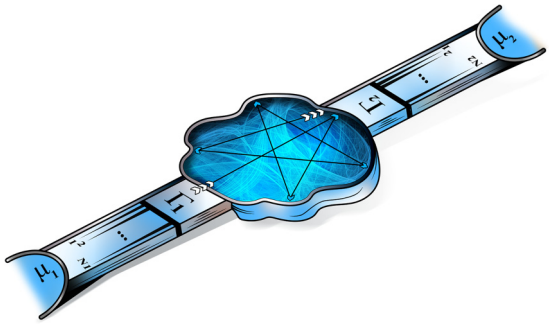

FIG. 1. Schematic view of the chaotic quantum dot in the universal regime coupled to two electron reservoirs through ideal leads, a paradigmatic mesoscopic system. Each lead contains N_i open channels, and the chaotic quantum dot (CQD) contains many resonances in the universal regime. As represented, in the ballistic regime, before exiting, the electron coherently collides many times with the edge of the CQD.

II. DERIVATION OF THE TUR FOR A QUANTUM DOT

Our starting point is establishing the connection between the charge current and its corresponding temporal fluctuations through thermodynamics uncertainty relations.

General formulation

We provide a complete analysis following Ref. [18] for charge transfer through a double-barrier chaotic quantum dot coupled to two leads, labeled as 1 and 2, with N_1 and N_2 open scattering channels, respectively. In addition, the system, schematically represented in Fig. 1, contains reservoirs with electrochemical potentials, μ_1 and μ_2, which are kept at an equilibrium temperature T. The tunneling rates Γ_i of the channel i can be controlled through changes in the gate voltage.

We now define creation (annihilation) operators for an incident electron in the chaotic cavity with total energy E in leads 1 and 2 as $a_{i1}^{\dagger}(E)$ $(a_{i1}(E))$ and $a_{i2}^{\dagger}(E)$ $(a_{i2}(E))$, respectively. The index i represents the transverse channel in the left and right lead. The creation (annihilation) operators obey the usual fermionic algebra and are independent in different channels. Similarly, we define the creation (annihilation) operators for an outgoing electron and denote them with the letter b. The operators a and b are related via the scattering matrix S:

$$\begin{pmatrix} b_{11} \\ \cdots \\ b_{1N_1} \\ b_{21} \\ \cdots \\ b_{2N_2} \end{pmatrix} = S \begin{pmatrix} a_{11} \\ \cdots \\ a_{1N_1} \\ a_{21} \\ \cdots \\ a_{2N_2} \end{pmatrix}. \tag{4}$$

The S matrix establishes a connection between the outgoing and incoming states. It has dimensions $(N_1 + N_2) \times (N_1 +$

N_2) and a block structure that reads as

$$S = \begin{pmatrix} r_{N_1\times N_1} & t'_{N_1\times N_2} \\ t_{N_2\times N_1} & r'_{N_2\times N_2} \end{pmatrix}, \tag{5}$$

where r, r' ($N_i \times N_i$) and t, t' ($N_i \times N_j, i \neq j$) are the quantum dot's reflection and transmission matrix blocks, respectively. The connection between the modes must preserve the unitarity of the matrix S, which is guaranteed by the charge conservation in the scattering process.

The scattering matrix offers a complete description of the charge-transfer process. It allows the extraction of electronic transport information so that we can directly infer the system's transport observable quantities once the S matrix is known. For instance, the current operator $\hat{j}_i(z,\mathcal{T})$ of the electron flow in the z longitudinal direction of a lead in a time $\mathcal{T}$ is expressed in terms of the field operators as

$$\hat{j}_i(z,\mathcal{T}) = \frac{\hbar e}{2im}\int dx_\perp \Big[\hat{\Psi}_i^\dagger(\vec{x},\mathcal{T})\Big(\frac{\partial}{\partial z}\hat{\Psi}_i(\vec{x},\mathcal{T})\Big) - \Big(\frac{\partial}{\partial z}\hat{\Psi}_i^\dagger(\vec{x},\mathcal{T})\Big)\hat{\Psi}_i(\vec{x},\mathcal{T})\Big], \tag{6}$$

where the field operators are defined as

$$\hat{\Psi}_i(\vec{x},\mathcal{T}) = \int dE e^{-iE\mathcal{T}/\hbar}\sum_{n=1}^{N_i(E)}\frac{\psi_{in}(\vec{x}_\perp)}{(2\pi\hbar v_{in}(E))^{1/2}} \times (a_{in}e^{ik_{in}z/\hbar} + b_{in}e^{-ik_{in}z/\hbar}), \tag{7}$$

with $\psi_{in}(\vec{x}_\perp)$ the ordinary first-quantization transversal wave functions of the corresponding lead, while $\vec{x}_\perp$ is the transversal coordinate over the lead, $k_{in} = (2m(E - E_{in}))^{1/2}$ is the wave vector, and $v_{in}(E)$ is the velocity of the corresponding electronic transversal mode. Assuming only the transport of electrons close to the Fermi energy, after some algebra we obtain

$$\hat{j}_i(z,t) = \frac{e}{2\pi\hbar}\sum_{\alpha,\beta}\sum_{m,n}\int dE dE' e^{i(E-E')t/\hbar} \times a^\dagger_{\alpha m}(E)\mathcal{J}^{mn}_{\alpha\beta}(i;E,E')a_{\beta n}(E'), \tag{8}$$

in which the Greek indexes α and β label the dot's incoming or outgoing waves, and the Latin ones denote the open channels in the respective leads. We have also defined the matrix $\mathcal{J}^{mn}_{\alpha\beta}(i;E,E') = \delta_{mn}\delta_{\alpha i}\delta_{\beta i} - \sum_k S^\dagger_{i\alpha;mk}(E)S_{i\beta;kn}(E')$. For a system at thermal equilibrium, the expected value of the product of creation and annihilation operators satisfies $\langle \hat{a}^\dagger_{\alpha m}(E)\hat{a}_{\beta n}(E')\rangle = \delta_{\alpha\beta}\delta_{mn}\delta(E-E')f_\alpha(E)$, where $f_\alpha(E)$ is the Fermi function. Therefore the time-average value of the current in the quantum dot is given by

$$\langle j\rangle = \frac{e}{2\pi\hbar}\int dE \mathrm{Tr}(t^\dagger(E)t(E))(f_1(E) - f_2(E)). \tag{9}$$

In the low-temperature limit, the above equation gives the remarkable Landauer-Büttiker formula for the conductance, $G = (e^2/2\pi\hbar)\mathrm{Tr}(t^\dagger(E_F)t(E_F))$.

The temporal, $\mathcal{T}$, current fluctuations are directly related to the fluctuation operator defined by $\Delta\hat{j}_\alpha(\mathcal{T}) = \hat{j}_\alpha(\mathcal{T}) - \langle\hat{j}_\alpha(\mathcal{T})\rangle$. Trivially, $\langle\Delta\hat{j}_\alpha(\mathcal{T})\rangle = 0$, i.e., the first relevant statistic for the fluctuation operator is in the symmetrized temporal correlation function:

$$\mathcal{P}_{\alpha\beta}(\mathcal{T}-\mathcal{T}') \equiv \tfrac{1}{2}\big\langle\Delta\hat{j}_\alpha(\mathcal{T})\Delta\hat{j}_\beta(\mathcal{T}') + \Delta\hat{j}_\beta(\mathcal{T}')\Delta\hat{j}_\alpha(\mathcal{T})\big\rangle. \tag{10}$$

For time-homogeneous correlation functions, the Fourier transform of the fluctuations of the current is

$$\Delta\hat{j}_{\alpha,\beta}(\mathcal{T}) = \frac{1}{2\pi}\int_{-\infty}^{\infty} d\omega \Delta j_{\alpha,\beta}(\omega)e^{i\omega t}, \tag{11}$$

which yields

$$2\pi\delta(\omega+\omega')\mathcal{P}_{\alpha\beta}(\omega) = \langle\Delta j_\alpha(\omega)\Delta j_\beta(\omega') + \Delta j_\beta(\omega')\Delta j_\alpha(\omega)\rangle. \tag{12}$$

The term $\mathcal{P}_{\alpha\beta}(\omega)$ is referred to as noise power. After some algebra involving second-quantization operators, we obtain the noise power at zero frequency,

$$\mathcal{P}_{\alpha\beta} = \frac{e^2}{2\pi\hbar}\sum_{\gamma\delta}\sum_{mn}\int dE \mathcal{J}^{mn}_{\gamma\delta}(\alpha;E,E)\mathcal{J}^{nm}_{\delta\gamma}(\beta;E,E) \times \big\{f_\gamma(E)[1-f_\delta(E)] + f_\delta(E)\big(1-f_\gamma(E)\big)\big\}, \tag{13}$$

where $\mathcal{P}_{\alpha\beta} \equiv \mathcal{P}_{\alpha\beta}(0)$. Due to current conservation, we obtain $\mathcal{P} \equiv \mathcal{P}_{11} = \mathcal{P}_{22} = -\mathcal{P}_{12} = -\mathcal{P}_{21}$. On the scale of potential and temperature differences, the transmission coefficients vary very weakly as a function of the Fermi energy. Therefore we can replace the values in the integrand with the Fermi energy, and we obtain

$$\mathcal{P}(T,eV) = \frac{e^2}{\pi\hbar}\Big[2k_BT\mathrm{Tr}(tt^\dagger) + eV\coth\Big(\frac{eV}{2k_BT}\Big)\mathrm{Tr}(tt^\dagger rr^\dagger)\Big]. \tag{14}$$

In the zero-temperature limit, the above equation becomes

$$\mathcal{P}(0,eV) = \frac{e^2}{\pi\hbar}\mathrm{Tr}(tt^\dagger rr^\dagger)e|V|, \tag{15}$$

which is known as the shot-noise power and has a purely quantum or corpuscular nature that is the central feature responsible for the quantum fluctuation of the electronic current. In the finite-temperature limit, thermal and quantum fluctuations compete.

The shot-noise power can also be interpreted as the variance associated with the temporal fluctuations of the current (charge transferred per unit time) $j(t) = GV$, in which G represents the conductance. Thus, $\langle\langle j^2\rangle\rangle \equiv \langle j^2\rangle - \langle j\rangle^2 = \mathcal{P}(T,eV)$. From now on, let us concentrate on the case of a universal quantum dot, Fig. 1. The TURs impose restrictions on the domain of possible values of thermodynamic currents (e.g., heat, particles, etc.). We start by considering $\mathcal{J}$ as being any current exchanged during a nonequilibrium process over a time interval. The TURs establish a relation between the steady-state current $\langle\mathcal{J}\rangle$, its time fluctuations $\langle\langle\mathcal{J}^2\rangle\rangle = \langle\mathcal{J}^2\rangle - \langle\mathcal{J}\rangle^2$, and the average entropy production rate $\langle\sigma\rangle$:

$$\frac{\langle\langle\mathcal{J}^2\rangle\rangle}{\langle\mathcal{J}\rangle^2}\frac{\langle\sigma\rangle}{k_B} \geqslant 2, \tag{16}$$

where k_B is the Boltzmann constant. Away from equilibrium, Eq. (16) points to a tradeoff between precision and dissipation, which means that a precise process with little noise is realized with a high entropic cost.

We now turn to the transport of stationary charge, denoted by j, which occurs in response to voltage V applied. And the dissipation is given by Joule's law,

$$\langle \sigma \rangle = \langle j \rangle \frac{V}{T}, \tag{17}$$

with T being the temperature of the electronic reservoirs. Combining Eqs. (17) and (16), we obtain the following expression:

$$\frac{V}{k_B T} \frac{\langle\langle j^2 \rangle\rangle}{\langle j \rangle} \geqslant 2. \tag{18}$$

It proves convenient to define the combination $Q \equiv \frac{V}{k_B T} \frac{\langle\langle j^2 \rangle\rangle}{\langle j \rangle}$, which is a function of both voltage and temperature. The Q factor is the observable interest of the TUR. We refer to systems that obey this inequality as "satisfying the TUR":

$$Q \geqslant 2. \tag{19}$$

TUR violations correspond to situations in which the left-hand side of Eq. (18) is smaller than 2.

While the entropy production σ is a non-negative deterministic quantity for macroscopic systems, it becomes random at the microscopic scale owing to the presence of non-negligible thermal and quantum fluctuations, present thermal and shot-noise, respectively. To gain some insight into the noise's physical meaning, we shall derive the TUR [35] in the limit of quantum coherence, defining the transmission eigenvalues τ_k (barriers) of the channel k. The electronic current and the shot noise, under the potential difference $\Delta\mu = eV$, are given by

$$\langle j \rangle = G_0 V \sum_i \tau_i, \tag{20}$$

$$\langle\langle j^2 \rangle\rangle = 2 k_B T G_0 \sum_i \tau_i^2 + G_0 \sum_i \tau_i (1 - \tau_i) \Delta\mu \coth\left(\frac{\Delta\mu}{2 k_B T}\right). \tag{21}$$

After some algebra we obtain

$$Q = \frac{\sum_i \tau_i (1 - \tau_i)}{\sum_i \tau_i} \left(\frac{\Delta\mu}{k_B T} \coth \frac{\Delta\mu}{2 k_B T} - 2 \right), \tag{22}$$

where $F = \sum_i \tau_i (1 - \tau_i) / \sum_i \tau_i$ is the Fano factor, and $G_0 = 2e^2/h$ is the quantum of conductance. We have also defined the quantities $\frac{\Delta\mu}{k_B T} \equiv \theta$ and $\theta \coth(\theta/2) - 2 \equiv f(\theta)$. Then, Eq. (22) can be written as

$$Q = F f(\theta) \geqslant 2. \tag{23}$$

In the universal regime, chaotic fluctuations arise, and averages of any transport observable depend solely on fundamental symmetries. Despite this, the theoretical description of the conductance, the shot-noise power, and the Fano factor are far from trivial. Notably, in the case of a few channels (extreme quantum regime), analytical results constitute a substantial technical challenge, and we remark that in the case of barriers' presence, the results are generally unknown. In the present study, therefore, we provide an analysis based on numerical simulation in the universal regime. In the next section we pedagogically develop the study and indicate the comparison with known analytical results.

III. SIMULATIONS OF THE UNIVERSAL RESONANT SCATTERING PROCESSES

We develop a numerical simulation through the Mahaux-Weidenmüller formulation [39]. The scattering matrix, written as a function of the Fermi energy ϵ and the Hamiltonian $\mathcal{H}$, describes the resonance states inside the ballistic chaotic quantum dot. The S matrix can be written as

$$S = 1 - 2i\pi \mathcal{W}^\dagger (\epsilon - \mathcal{H} - i\pi \mathcal{W}\mathcal{W}^\dagger)^{-1} \mathcal{W}, \tag{24}$$

where $\mathcal{W}$ is a deterministic matrix describing the interaction between the CQD's resonant states and the leads' propagating channels.

The numerical simulation performed in this work generates an ensemble of random Hamiltonians using the framework of RMT. As a statistical theory of spectra, the RMT concatenate the CQD fundamental symmetries with their energy eigenvalue distribution. Initially observed by Wigner and Dyson, the Hamiltonian of the chaotic cavity is classified by the presence or/and absence of time-reversal (TRS) and spin-rotation symmetries (SRS).

The coupling of the resonance states with the propagating modes in the leads is carried out using the deterministic matrix $\mathcal{W} = (\mathcal{W}_1, \mathcal{W}_2)$. The matrix $\mathcal{W}$ can be decomposed into two sub-blocks $(\mathcal{W}_1)_{M \times N_1}$ and $(\mathcal{W}_2)_{M \times N_2}$, which describe the interaction of the QD's M resonances with N_i channels. The transmission via the resonant QD occurs without direct processes, i.e., the electron cannot change channels without going through some resonance. Therefore the deterministic matrix satisfies the orthogonality condition

$$\mathcal{W}_\alpha^\dagger \mathcal{W}_\beta = \gamma_\alpha \frac{N\Delta}{\pi^2} \delta_{\alpha\beta},$$

which Δ is the average spacing between consecutive resonant levels. The diagonal γ_α matrix is associated with the transmission probabilities $\Gamma_{\alpha,a} \in [0, 1]$, and it can be written as $\gamma_\alpha = \mathrm{diag}(\gamma_{\alpha,1}, \ldots, \gamma_{\alpha N})$. The barriers (tunneling probabilities) are related to $\gamma_{\alpha a}$ through the relation $\Gamma_{\alpha a} = \mathrm{sech}^2[-\ln(\gamma_{\alpha a})/2]$. In this study, for the sake of simplicity, we consider identical couplings in each lead, i.e., when $\Gamma_\alpha = \Gamma_{\alpha i}, \forall i$. The barriers are generically known as ideal if $\Gamma = 1$ (total electronic tunneling), and it is opaque if $\Gamma \to 0$ (electronic tunneling with probability tending to zero). Barriers can be physically realized through contacts, CQD input constrictions, or a voltage gate [40–44].

In the framework of random-matrix theory, the Schrödinger billiard has Hamiltonian belonging to the Wigner-Dyson ensemble whose elements are independent random numbers and have a probability distribution $\mathcal{F}$ of the form [45]

$$\mathcal{F}(\mathcal{H}) \propto \exp\left(-\frac{\beta M}{4\lambda^2} \mathrm{Tr}(\mathcal{H}^\dagger \mathcal{H}) \right), \tag{25}$$

in which $\lambda = M\Delta/\pi$ is the variance related to the electronic single-particle mean level spacing Δ, and M is the resonances of the chaotic cavity. The $\beta = 1, 2, 4$ is Dyson's symmetry index, and they designate, respectively, the Gaussian orthogonal ensemble (GOE), the Gaussian unitary ensemble (GUE), and the Gaussian symplectic ensemble (GSE). The $\beta = 1$ index symmetry describes systems that preserve the TRS and SRS. Mathematically, the GOE is represented by an ensemble of real and symmetric random Hamiltonian matrices. The unitary ensemble (GUE), with index $\beta = 2$, describes systems that violate the TRS, and complex matrix elements give its Hamiltonian representation. Finally, the GSE, $\beta = 4$, is for systems that violate the SRS but preserve the TRS. Hamiltonians with symplectic structure represent the GSE ensemble $\mathcal{H} = a\mathbf{1} + i(b\sigma_x + c\sigma_y + d\sigma_z)$, with σ_i denoting the Pauli matrices.

In addition to Schrödinger's billiard, the Dirac billiard is a CQD performed using graphene or topological insulators [46] and thereby supports the chiral/sublattice symmetry such that its ensembles members satisfy [47]

$$\mathcal{H} = -\Sigma_z \mathcal{H} \Sigma_z;\ \Sigma_z \equiv \sigma_z \otimes \mathbf{1}_M = \begin{pmatrix} \mathbf{1}_M & \mathbf{0}_M \\ \mathbf{0}_M & -\mathbf{1}_M \end{pmatrix},$$

from which we deduce that their Hamiltonians can be represented as antidiagonal arrays with the double order

$$\mathcal{H} = \begin{pmatrix} 0 & \mathcal{C} \\ \mathcal{C}^\dagger & 0 \end{pmatrix}.$$

Thus, the Hamiltonian blocks admit Gaussian distributions given by

$$\mathcal{F}(\mathcal{C}) \propto \exp\left(-\frac{\beta M}{4\lambda^2}\mathrm{Tr}(\mathcal{C}^2)\right),$$

where the index $\beta = 1, 2, 4$ describes, respectively, the GOE chiral ensemble (chGOE), the GUE chiral ensemble (chGUE), and the GSE chiral ensemble (chGSE). To ensure the chaotic regime and universality, the number of resonances inside the quantum dot is large, $M = 400$.

For pedagogical reasons, our starting point is the numerical simulation of the average conductance in the ensemble, $[G]/G_0$. The conductance in mesoscopic systems at zero temperature is $G/G_0 \equiv \mathrm{Tr}(t^\dagger t)$, and we obtain its ensemble average over the Hamiltonian realizations. In the universal regime, the averages are isospectral, i.e., we can execute them by setting the energy as zero for simplicity, $\epsilon = 0$. In addition, we perform a numerical simulation of the average shot-noise power in the ensemble, $[\mathcal{P}]/\mathcal{P}_0$, where the shot-noise power can be obtained by $\mathcal{P}/\mathcal{P}_0 = \mathrm{Tr}(t^\dagger t\ (1 - t^\dagger t))$, also taking $\epsilon = 0$. At the same time, we will consider $\mathcal{P}$ as the noise amplitude temporal average for each realization. We depict the behavior of the two observable for the three Wigner-Dyson (WD) symmetries and the three chiral (Dirac) symmetries, respectively, in Figs. 2(a), 2(c), 3(a), and 3(c) for the extreme quantum regime ($N = 1$), recovering the results of Ref. [48]. Even though conductance is monotonically increasing as a function of the barrier for all WD universal symmetries, surprisingly, it presents a highly non-Ohmic and completely distinct behavior in all cases. According to the known analytical results for the WD universality classes, the average conductance in the

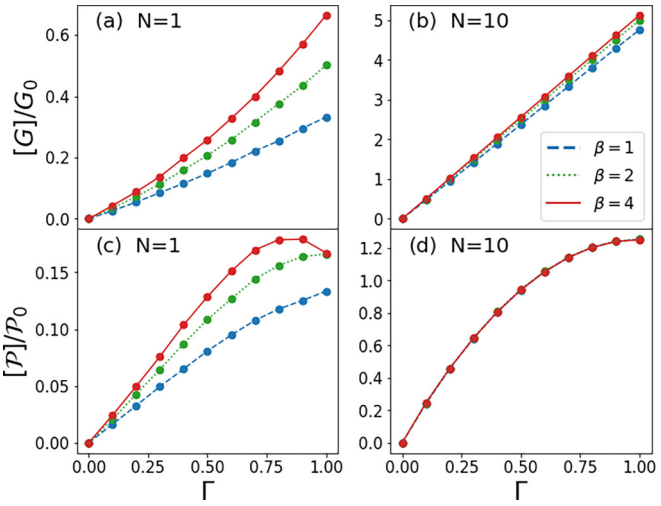

FIG. 2. The ensemble average of the conductance and the shot-noise power for Wigner-Dyson symmetry classes.

mesoscopic regime is given by [49]

$$\frac{[G]}{G_0} = \frac{G_1 G_2}{G_1 + G_2}\left(1 + \left(1 - \frac{2}{\beta}\right)\frac{G_2\Gamma_1 + G_1\Gamma_2}{(G_1 + G_2)^2}\right), \quad (26)$$

where $G_i = \Gamma_i N_i$ for $i = 1, 2$. The first term is the dominant semiclassical contribution, agreeing with Ohm's law. The second term is the weak-localization (WL) correction, i.e., electronic transport's main quantum interference correction (QIC) in disordered many-body systems.

In the case of $N = 1$, Eq. (26) yields $[G]/G_0 = \Gamma/2(1 + 1/2(1 - 2/\beta))$, i.e., the analytical result provides a linear behavior in Γ (Ohmic); nevertheless, the analytical result is valid only in the semiclassical regime, $N \gg 1$. Therefore the extreme quantum regime is highly non-Ohmic due to high-order quantum interference corrections. In addition, graphene quantum dots (chiral systems) present a transition both in the conductance and in the shot-noise power, for which the values of the two pure ensembles, orthogonal and symplectic,

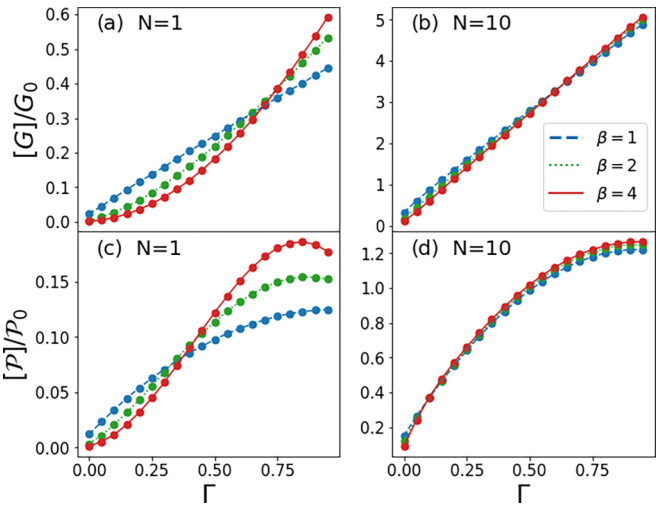

FIG. 3. The ensemble average of the conductance and the shot-noise power for chiral (Dirac) symmetry classes.

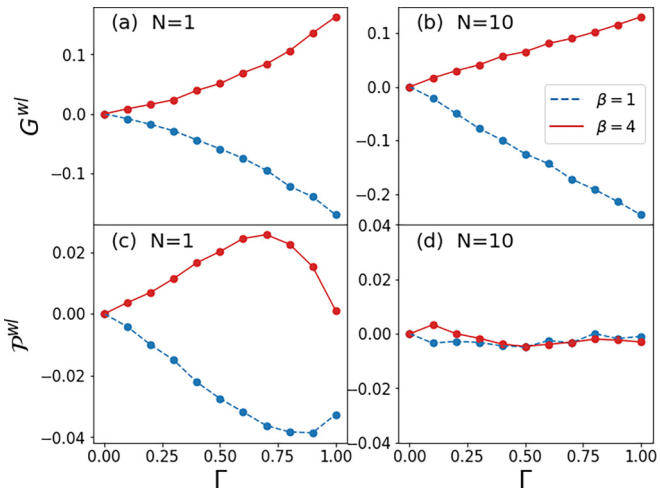

FIG. 4. The localization term of conductance and shot-noise power for Wigner-Dyson classes.

intersect as a function of the barriers, as demonstrated in Figs. 3(a) and 3(b).

In the semiclassical regime, $N = 10$, the results for the three Wigner-Dyson and chiral universality classes are depicted in Figs. 2(b), 2(d), 3(b), and 3(d), respectively. Notice, as expected, the Ohmic behavior in all conductance curves. In the chiral systems there is a transition in the signal of the quantum interference correction as a function of the barrier; specifically on the noise signal, notice that the QIC differentiates the three chiral ensembles and therefore carries the signature of the chirality, Fig. 5.

We have developed a method to extract the QIC of transport observable. The unitary class describes systems with broken time-reversal symmetry, i.e., it eliminates quantum interference correction. On the one hand, the unitary class supports only the semiclassical term of any observable. On the other hand, orthogonal and symplectic classes hold both the semiclassical and QIC terms, which means that to obtain interference corrections, we need to subtract the average of the

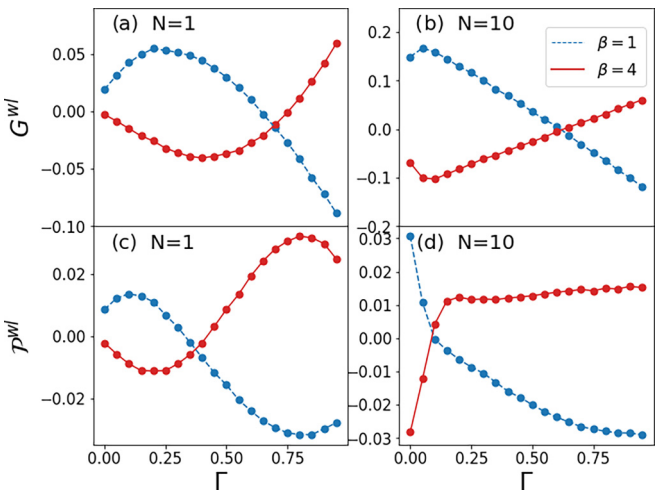

FIG. 5. The localization term of conductance and shot-noise power for chiral classes.

observable O in the orthogonal ($\beta = 1$) or symplectic ($\beta = 4$) classes from the average of the same observable in the unitary class ($\beta = 2$):

$$O^{\mathrm{QIC}} = O_{\beta=i} - O_{\beta=2}, \ i = 1 \text{ or } 4. \tag{27}$$

In Fig. 4 we can observe that the quantum interference sector for both the conductance and the shot-noise power is always positive and negative for the symplectic and orthogonal Wigner-Dyson classes, respectively. These phenomena are called weak antilocalization (positive) and weak localization (negative) [33]. It expresses how the symmetries alter the electronic path and its quantum properties, such as conductance and shot-noise power.

Unlike what happens with the WD universality classes, there are signal changes in the quantum interference corrections of the chiral classes, as depicted in Fig. 5. These transitions support the previous results for conductance and shot-noise power and reveal the crucial role of quantum interference in transport observables in the chiral classes, both from the point of view of the signal changes and magnitude when compared to the semiclassical term. Therefore the quantum interference correction can carry a relevant experimental signal for chirality signatures in graphene or topological insulators. This endeavor is a quest that begins in nuclear physics and elementary particle physics, and it is still a substantial challenge.

As mentioned before, these results would make it necessary to calculate the signal-to-noise ratio $Q_{\mathrm{TUR-MS}}$, defined as

$$Q_{\mathrm{TUR-MS}} = \frac{V}{k_B T} \frac{[\langle \mathcal{P} \rangle]}{[\langle G \rangle]}. \tag{28}$$

To calculate $Q_{\mathrm{TUR-MS}}$, the shot-noise power $\mathcal{P}/\mathcal{P}_0 = \mathrm{Tr}[t^\dagger t \ (1 - t^\dagger t)]$ and the conductance $G/G_0 \equiv \mathrm{Tr}(t^\dagger t)$ are averaged separately over a Hamiltonian ensemble. Thus we obtain the ratio $[\langle \mathcal{P} \rangle]/[\langle G \rangle]$. However, the $Q_{\mathrm{TUR-R}}$ is obtained by dividing the shot-noise power and the conductance before averaging it:

$$Q_{\mathrm{TUR-R}} = \frac{V}{k_B T} \left[\frac{\langle \mathcal{P} \rangle}{\langle G \rangle} \right]. \tag{29}$$

From this perspective our motivation for defining the $Q_{\mathrm{TUR-R}}$ is to treat the signal-to-noise ratio coefficient $\langle \mathcal{P} \rangle / \langle G \rangle$ as an intrinsic physical property of the system, such as conductance or shot-noise power $\mathcal{P}$, so that we could obtain, for instance, their respective statistical cumulants. In the simulation, each Hamiltonian of the ensemble provides a conductance $\langle G \rangle / G_0$, shot-noise power $\langle \mathcal{P} \rangle / \mathcal{P}_0$, and signal-to-noise ratio coefficient $\langle \mathcal{P} \rangle / \langle G \rangle$. Therefore, by averaging over the ensemble, for instance, in Fig. 6, we depict the signal-to-noise ratio, $[\langle \mathcal{P} \rangle / \langle G \rangle]$ (TUR-R) and $[\langle \mathcal{P} \rangle]/[\langle G \rangle]$ (TUR-MS), as a function of Γ for the relevant chiral chaotic billiard. Figure 6 displays two relevant regimes. The first shows the behavior of the TURs in the extreme quantum regime (few open channels), Fig. 6(a). The second one shows the result in the semiclassical regime (many open channels), Fig. 6(b). The shot-noise power is enhanced by tunneling ($\Gamma \to 0$), and consequently, both $Q_{\mathrm{TUR-R}}$ and $Q_{\mathrm{TUR-MS}}$ increase as Γ goes to zero. In this regime the eigenvalues τ_i of the transmission matrix $tt^\dagger$ go to zero in such a way that the signal-to-noise ratio $\sum_{i=1}^{N} \tau_i(1 - \tau_i) / \sum_{j=1}^{N} \tau_j$

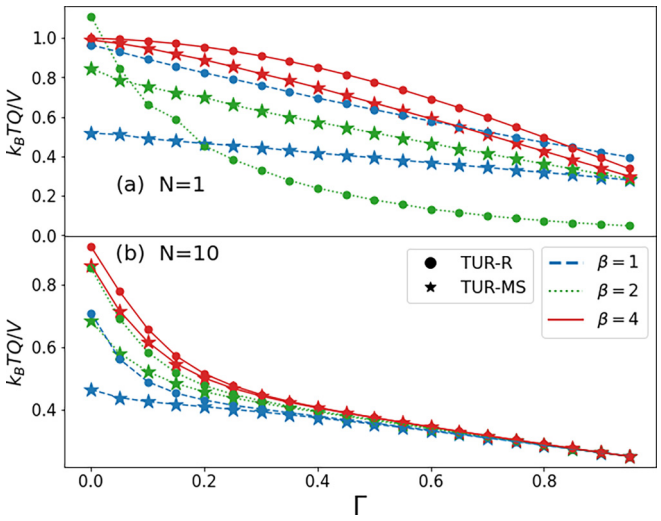

FIG. 6. The ensemble average of k_BTQ/V for both the main term of the TUR-R, Eq. (2), and the TUR-MS, Eq. (3), as a function of Γ for the chiral billiard, (a) for the $N = 1$ extreme quantum regime and (b) $N = 10$ semiclassical regime.

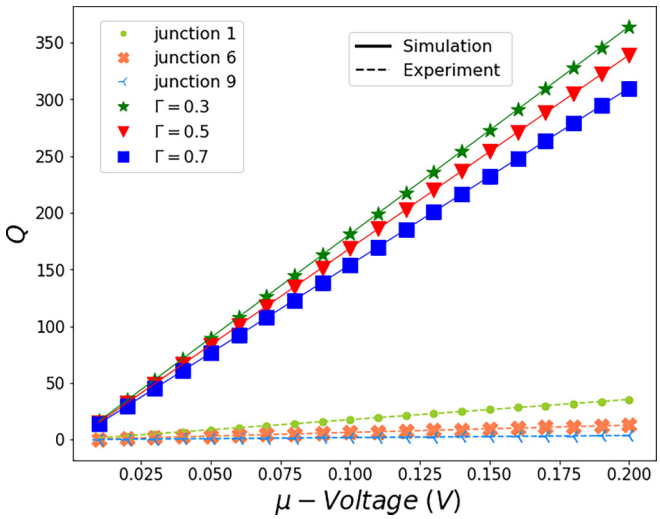

FIG. 7. TUR as a function of voltage in the extreme quantum regime. We compare a tunneling junction system's experimental data [35] with our QD simulation. Physically, a large number of resonant states in the chaotic cavity amplifies the signal-to-noise ratio when compared with junctions. The investigation shows that CQDs do not violate the TUR for all values of N and Γ according to the equation $Q \geqslant 2$ [Eq. (19)].

remains finite for both $Q_{\mathrm{TUR-R}}$ and $Q_{\mathrm{TUR-MS}}$. The values are different in the extreme quantum regime, which is indeed expected. However, surprisingly, the results are also different in the semiclassical regime in large intervals of barrier values, which characterizes a violation of the law of large numbers and the central limit theorem [as we can see in Fig. 6(b)].

IV. GENERALIZED TUR

As previously mentioned, the thermodynamic uncertainty relations (TURs) provide a tradeoff between fluctuations and entropy cost. The generalized version of the TUR was carried out in Ref. [25] and obtained by evaluating the minimum and saturable matrix derived from the fluctuation theorems (FTs). The generalized TUR is valid for systems in the extreme quantum and semiclassical regime subjected to processes that occur in a finite and nonstationary time. The generalized TUR, for any current $\mathcal{J}$, can be written as

$$\frac{\langle\langle \mathcal{J}^2\rangle\rangle}{\langle \mathcal{J}\rangle^2} \geqslant f\left(\frac{\langle\sigma\rangle}{k_B}\right), \tag{30}$$

where $f(x) = \mathrm{csch}^2[g(x/2)]$, $g(x)$ is the function inverse of $x\tanh(x)$, and $x = \langle\sigma\rangle/k_B$. Considering a charge current j and the shot noise under the potential difference $\delta\mu$, after some algebra we obtain

$$\frac{\langle\langle j^2\rangle\rangle}{\langle j\rangle^2} \geqslant f\left(\tfrac{V}{k_BT}\langle j\rangle\right) \rightarrow \tfrac{V}{k_BT}\tfrac{\langle\langle j^2\rangle\rangle}{\langle j\rangle} \geqslant \tfrac{V}{k_BT} f\left(\tfrac{V}{k_BT}\langle j\rangle\right).$$

Therefore

$$Q \geqslant \frac{V}{k_BT}\langle j\rangle f\left(\frac{V}{k_BT}\langle j\rangle\right). \tag{31}$$

A quantum dot is the simplest mesoscopic device, and it is particularly relevant for investigating the behavior of TUR, i.e., how the interference phenomenon competes with the thermal fluctuations. However, when we try to establish such an analysis for the generalized TUR, we notice that the representative numbers of the constants make the correction contribution incipient: $\theta = eV/k_BT$, where $e = 1.6 \times 10^{-19}$ C, $V \approx 10^{-3}$ V, $k_B = 1.38 \times 10^{-23}$ m^2 kg s^{-2} K^{-1}, $T = 10$ K, and $G_0 \approx 7.74 \times 10^{-5}$ S. These values make x very large; consequently, $f(x) = \mathrm{cosech}^2(x)$ assumes very small values, on the order of 10^{-12}. Therefore the QIC contribution will always be much more significant than the thermal correction.

V. TUR's GIANT QUANTUM INTERFERENCE CORRECTION

Surprisingly, the previous results suggest that the dominant correction of thermodynamic observables comes from quantum interference, even in the semiclassical regime. In the extreme quantum regime, quantum interference has dramatic manifestations in the transport properties, which is much more relevant than in the semiclassical regime. This fact motivates extensive analysis of the current section.

Firstly, if $N_1 = N_2 = 1$, in Fig. 7 we depict three curves using our extreme quantum limit simulation data for an ensemble of CQD and three curves from experiment data using an Au atomic-scale junction [35]. The curves from simulation for $\Gamma = 0.3$, $\Gamma = 0.5$, and $\Gamma = 0.7$ correspond to ensemble-averaged Fano factors with values of 0.9147, 0.8517, and 0.7785, respectively. On the other hand, the curves from the experiment involving an Au atomic-scale junction correspond to constant Fano factors of 0.089 (junction 1), 0.032 (junction 6), and 0.0091 (junction 9). Figure 7 is a graph obtained for $T = 6.0$ K. There is an order-of-magnitude difference when comparing the results of a CQD with those of an experimentally measured tunneling (constriction) junction. Consequently, our result reflects the signal amplification in the CQD that, unlike a constriction, supports quantum interference mechanisms. Physically, the signal-to-noise ratio is

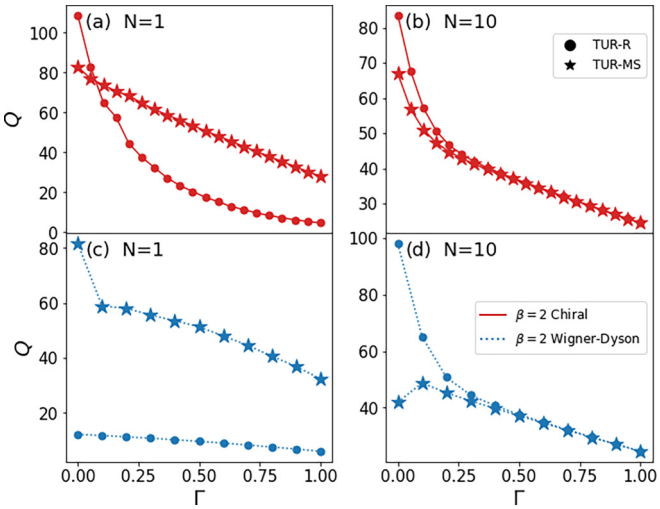

FIG. 8. TUR-R and TUR-MS calculated for the Fano factor values of the unitary class. We performed $\mu = 0.05$ V and $\beta \equiv 1/k_BT \sim 2000$ eV^{-1}. According to the equation $Q \geqslant 2$ [Eq. (19)], both TUR-R and TUR-MS satisfy the TUR condition.

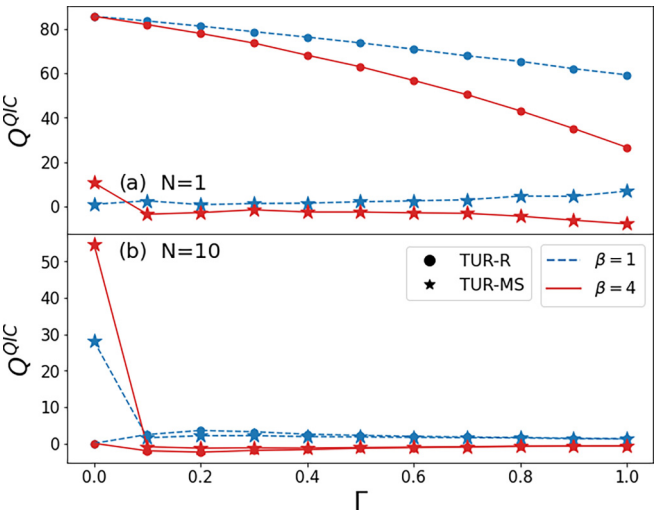

FIG. 9. The quantum interference correction (QIC) of the TUR-R and TUR-MS calculated for the Fano factor values of the orthogonal and symplectic Wigner-Dyson symmetry classes. We perform $\mu = 0.05$ V and $(k_BT)^{-1} \sim 2000$ eV^{-1}.

substantially more significant in a ballistic CQD than in a junction because of increased shot noise. As a charge current fluctuation quantifier, the shot noise increases as the amount of electron paths increases in a mesoscopic system. These paths are directly related to the accessible states inside the scattering cavity, which are the resonant eigenvalues of the Hamiltonian.

Until now, we have discussed the physical meaning of the TUR and its difference in quantum systems, such as the quantum dot with one or few resonances, and our mesoscopic device, the CQD or billiard, with a large number of resonances. From now on, we present the influence of the tunneling barrier on the signal-to-noise factor in both representations, $\mathcal{Q}_{\mathrm{TUR-R}}$ and $\mathcal{Q}_{\mathrm{TUR-MS}}$. In Fig. 8 is depicted the TUR factor for the unitary class, which demonstrates the crucial role of tunneling barriers (symmetric). In the extreme quantum regime ($N = 1$), notice that the value of the TUR-R $\mathcal{Q}_{\mathrm{TUR-R}} = [\langle\mathcal{P}\rangle/\langle G\rangle]$, represented by balls in Fig. 8, differs significantly from the well-known, by literature, TUR-MS $\mathcal{Q}_{\mathrm{TUR-MS}} = [\langle\mathcal{P}\rangle]/[\langle G\rangle]$, represented by stars in Fig. 8, for both WD [Fig. 8(a)] and chiral [Fig. 8(c)] universality classes. In the extreme quantum regime, there is a significant divergence between TUR-R and TUR-MS, regardless of fundamental symmetry. Another striking feature is, although one can observe a convergence of the TUR-R and TUR-MS in the semiclassical regime, as expected, there is a divergence for low values of the Γ in the WD unitary class when the central limit theorem (CLT) would be valid.

A. Chaotic quantum dots of Schrödinger

Going forward, we analyze the WD universality classes (orthogonal and symplectic) considering $\delta\mu = 0.05$, and we obtain the TUR interference term separately, $\mathcal{Q}^{\mathrm{QIC}}$. We aim to analyze how TUR factors $\mathcal{Q}_{\mathrm{TUR-R}}$ and $\mathcal{Q}_{\mathrm{TUR-MS}}$ behave when fundamental symmetries are preserved. In particular, we are interested in how TUR factors can distinguish the presence and/or absence of fundamental symmetries by analyzing the QIC. In Fig. 9 we depict the behavior of that term, i.e., when only the QIC in the Fano factor is taken into account. There is a comparison in Fig. 9 between the QIC of the TUR in the extreme quantum limit with the Fano factor, written as $[\langle\mathcal{P}\rangle]/[\langle G\rangle]$ and $[\langle\mathcal{P}\rangle/\langle G\rangle]$.

One can note a discrepancy between the two results under the same conditions at the extreme quantum limit. At the same time, there is a coincidence in the semiclassical regime for sufficiently high values of the barriers. In the quantum regime the result shows that only the TUR-R presents a significant QIC, indicating that the TUR-R is more sensitive to fundamental symmetries than the TUR-MS. In the semiclassical regime, the QIC becomes more imperceptible, making $\mathcal{Q}^{\mathrm{QIC}}$ go to zero for both factors, $\mathcal{Q}_{\mathrm{TUR-R}}$ and $\mathcal{Q}_{\mathrm{TUR-MS}}$. Moreover, the fact that QIC for both factors tends to be equal in a semiclassical regime demonstrates the unfolding of the CLT for some transparency barrier Γ values.

There are known situations in the literature where averages of ratios of stochastic variables are ill-defined, i.e., they diverge due to division by numbers arbitrarily close to zero with nonzero probability. One such situation is the efficiency, defined as $\langle$(output work)/(input heat)$\rangle$, as can be seen in Ref. [50]. Indeed, variables of the form $[X/Y]$ can be potentially problematic. However, we have carefully examined the situation and determined that, in our specific case, these issues can be safely disregarded.

We can observe that the total $\mathcal{Q}$ factors consist of the sum of the semiclassical (SC) and QIC terms, i.e., $\mathcal{Q} = \mathcal{Q}^{\mathrm{SC}} + \mathcal{Q}^{\mathrm{QIC}}$. Comparing the results depicted in Fig. 9 with those in Fig. 10, it is found that, surprisingly, the QIC term of quantum corrections is the dominant one, which leads one to conclude that the QIC is the main contribution to the validity of TUR-R for some regimes. Table I shows some values of $\mathcal{Q}$ for various regimes for ideal contacts, $\Gamma = 1$. For the Wigner-Dyson (WD) classes, observe that $\mathcal{Q}^{\mathrm{QIC}}/\mathcal{Q}$ reaches 90% of the total contribution to the TUR-R in the orthogonal universal class. In comparison, the value in this same regime yields 18.5%

TABLE I. (Ideal barriers, $\Gamma = 1.0$) In the first two lines we show the quantitative differences between the two types of observable associated with TUR in CQDs. In the third line we discriminate the experimental data obtained through Au tunneling junctions and show the differences in their values compared to CQDs in any universal symmetry. The quantum interference contribution, Q^{QIC}, the total value, Q, and the percentage interference contribution, Q^{QIC}/Q, are indicated in the last three columns, respectively. Notice the violation of the central limit theorem (CLT), the chirality fingerprint, and the role of the number of open channels in the TUR.

	Class	Ensemble	Junction (Fano factor)	Q^{QIC} $N=1; N=10$	Q $N=1; N=10$	$\frac{Q^{\mathrm{QIC}}}{Q}$ % $N=1; N=10$
$Q_{\mathrm{TUR\text{-}R}}$ (CQD)	Wigner-Dyson	Orthogonal	–	58.90; 1.28	65.38; 25.91	90.0; 4.94%
		Symplectic	–	26.80; −0.71	32.66; 23.91	82.0; 2.96%
	Chiral	Orthogonal	–	34.20; 0.04	38.74; 24.59	88.2; 0.1%
		Symplectic	–	27.8; −0.013	33.10; 24.53	83.9; 0.05%
$Q_{\mathrm{TUR\text{-}MS}}$ (CQD)	Wigner-Dyson	Orthogonal	–	7.3; 1.20	39.26; 25.78	18.5; 4.65%
		Symplectic	–	−7.9; −0.66	24.81; 23.89	31.84; 2.76%
	Chiral	Orthogonal	–	−0.58; 0.01	27.45; 24.53	2.11; 0.04%
		Symplectic	–	1.34; 0.002	29.33; 24.52	4.56; 0.08%
$Q_{\mathrm{TUR\text{-}MS}}$ (Junction)	–	–	Junction 1 (0.089)	–	3.16	–
	–	–	Junction 6 (0.032)	–	8.57	–
	–	–	Junction 9 (0.010)	–	1.00	–

for the TUR-MS; that is, the TUR factor developed in this investigation is much more sensitive from a quantum point of view. Similar results are observed in the symplectic class of WD. In Table II we observe effects of the same magnitude for the WD symmetry classes in the opaque regime, indicating the TUR-R's robustness. It is pertinent to emphasize that the present investigation reveals that, for all values of N and Γ, the quantity Q exhibits values greater than 2 for both TURs, as depicted in all the figures involving the Q factors. Therefore it can be inferred, based on Eq. (19), that none of the studied (Wigner-Dyson or chiral) CQDs violate the TUR.

As mentioned, in the quantum regime the TUR-MS does not present a significant Q^{QIC} term in the WD ensembles, as one can see in Fig. 9 and Tables I and II for $N = 1$. Hence the $Q_{\mathrm{TUR-MS}}$ in Fig. 10 is constituted, in most cases, of more than 90% semiclassical origin. Therefore, if we used the results of TUR-MS, we would infer that fundamental symmetries do not have a crucial role in the QIC for the TUR-MS, unlike the TUR-R. Consequently, in the extreme quantum regime, the discrepancy observed between the ballistic CQD simulation and the experimental data for a tunneling junction, depicted in Fig. 7, could be explained by the quantum interference contribution that amplifies the Q factor signal by 10 orders of magnitude. Accordingly, quantum interference is the echo of the ballistic chaotic quantum dot associated with accessible states inside the cavity when compared to a constriction. Thus, the QIC has proved to be a substantial source of information on the underlying dynamics in finite-size systems. Finally, as $Q_{\mathrm{TUR-R}} \approx Q_{\mathrm{TUR-MS}}$ in the semi-classical regime (a large number of open channels), we remark on the validity of the CLT, as shown in Fig. 10.

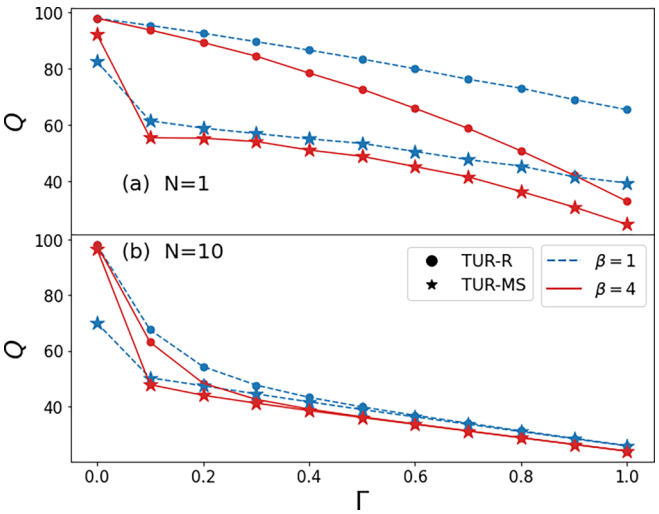

FIG. 10. TUR-R and TUR-MS calculated for the Fano factor values of the orthogonal and symplectic Wigner-Dyson symmetry classes. We perform $\mu = 0.05$ V and the $(k_B T)^{-1} \sim 2000\ \mathrm{eV}^{-1}$. According to the equation $Q \geqslant 2$ [Eq. (19)]), both TUR-R and TUR-MS satisfy the TUR condition.

B. Chaotic quantum dots of Dirac

We now turn to the chiral universality classes (chOrthogonal and chSymplectic), where all analyses were performed through average in ensembles containing 10^4 realizations. To put it in context, theoretical studies of graphene billiards allowed engendering effective Dirac models, i.e., relativistic quantum mechanics. Early studies have already revealed that graphene CQD billiards have a behavior dictated by two copies of mutually coupled "neutrino" billiards. Although relevant from a theoretical point of view, the experimental signal of chirality from neutrino physics remains a significant challenge, both in elementary particle physics and in condensed-matter physics labs. Here we propose the TUR-R signal as a strong fingerprint of chirality. As in the WD ensembles, we find an unexpected divergence between $[\mathcal{P}]/[G]$ and $[\mathcal{P}/G]$ for both the Q^{QIC} and Q factor in the extreme quantum regime. In Fig. 11 we show the behavior of the Q^{QIC} factor for chiral universality classes. For sufficiently high values of Γ, the quantum interference effect is remarkable in the extreme quantum limit, whereas it is low in the semiclassical regime.

TABLE II. (The opaque regime, $\Gamma = 0.1$) In the lines we show the quantitative differences between the two types of observable associated with TUR in CQDs in any universal symmetry. The quantum interference contribution, Q^{QIC}, the total value, Q, and the percentage interference contribution, Q^{QIC}/Q, are indicated in the last three columns, respectively. Notice the violation of the central limit theorem (CLT), the chirality fingerprint, and the role of the number of open channels in the TUR.

	Ensembles	Class	Q^{QIC} $N=1;N=10$	Q $N=1;N=10$	$\frac{Q^{\mathrm{QIC}}}{Q}$ % $N=1;N=10$
$Q_{\mathrm{TUR\text{-}R}}$ (CQD)	Wigner-Dyson	Orthogonal	83.0; 2.39	95.31; 67.33	87.08; 3.54%
		Simpletic	81.7; −2.06	93.76; 63.0	87.13; 3.27%
	Chiral	Orthogonal	22.0; −9.30	87.1; 47.9	25.2; 19.41%
		Simplectic	30.9; 7.21	95.6; 64.37	32.33; 11.2%
$Q_{\mathrm{TUR\text{-}MS}}$ (CQD)	Wigner-Dyson	Orthogonal	2.90; 1.52	61.43; 50.28	4.72; 3.02%
		Simpletic	−3.3; −0.92	55.35; 47.77	5.96; 1.92%
	Chiral	Orthogonal	−26.0; −9.30	48.2; 41.61	53.94; 22.35%
		Simplectic	18.7; 9.21	92.8; 60.2	20.15; 15.3%

Similarly to the Wigner-Dyson symmetry classes, the quantum interference correction is more expressive in the TUR-R than in the TUR-MS for most barrier transparency Γ values. In particular, for the ideal case of the transparent barrier $\Gamma = 1$, the TUR-MS does not present any contribution to the quantum interference, unlike the TUR-R. Thus the TUR-MS would not be efficient in distinguishing fundamental symmetries by QIC, the same as the TUR-R. For the semiclassical regime, like WD quantum dots, chirality depletes TUR interference contributions as the system goes to the transparent barrier case $\Gamma = 1$. Analogous to the Wigner-Dyson quantum dot, quantum interference corrections become imperceptible in a semiclassical regime for chiral symmetries. In Table I, some Q values are explored for a myriad of regimes for ideal contacts, $\Gamma = 1$. For the chiral classes, observe that Q^{QIC}/Q reaches 88.2% of the total contribution to the TUR-R in the orthogonal universal class. In comparison, the value in this same regime yields 2.11% for the TUR-MS; the TUR factor developed in this investigation is much more sensitive from a quantum point of view. Similar results are observed in the symplectic class of Dirac. In Table II we observe effects of the same magnitude for the Dirac symmetry classes in the opaque regime, indicating the TUR-R's robustness.

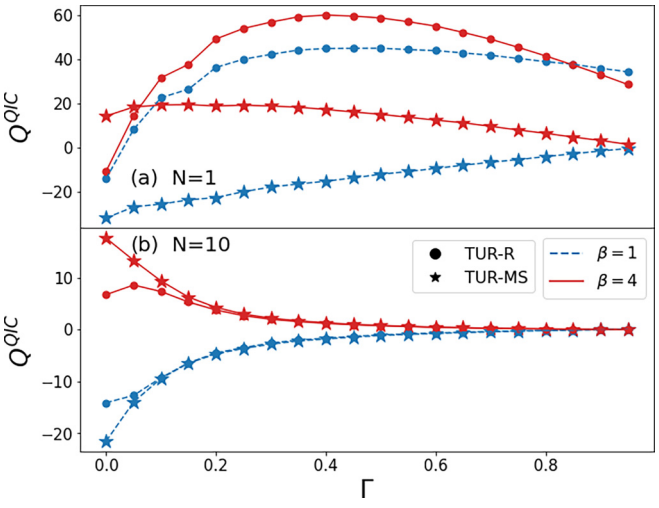

FIG. 11. The quantum interference correction (QIC) of the TUR-R and TUR-MS was calculated for the Fano factor values of the ChOrthogonal and ChSymplectic chiral symmetry classes. We perform $\mu = 0.05$ V and $\beta \equiv 1/k_B T \sim 2000\ \mathrm{eV}^{-1}$.

In the search for "chiral neutrinos," theoretical studies indicate that chirality is a subtle signal that disappears in several ways. Specifically in CQD, it is known that this signal is not detectable for more than $N = 2$ open channels. Notice in Table I that the signal of chirality disappears as the number of open channels increases. However, when comparing the results shown in Table I with those in Table II, a remarkable finding appears: the chirality signal is amplified from 0.04% to 22.35% if there are many open channels ($N = 10$), as long as the regime is opaque, that is, the chirality signal does not disappear for the TUR parameters even in the semiclassical regime. The same does not occur for the Wigner-Dyson classes. Therefore here we describe a way to detect the chirality signal with a very high amplification margin in graphene CQD billiards.

In addition, one notes that there is a quantum correction amplification-depletion transition in the extreme quantum regime as the barrier values tend towards the opaque limit. This fact is associated with the unusual behavior of the QIC for chiral quantum dots. Unlike the CQD governed by Wigner-Dyson ensemble classes, in Fig. 5 we can observe that the system presents localization and antilocalization corrections depending on the barrier transparency value Γ. Thus, this change in the sign of weak localization (Fig. 5) can best be seen in the way in which the TUR-R changes the sign of its derivative as Γ increases [see Fig. 11(a)], unlike the TUR-MS. Therefore these changes in the sign of derivative would not be seen by independent observations of the shot-noise power and conductance averages. We note that the effect is not present in the semiclassical regime in which both symplectic and orthogonal symmetry yields monotonous dependence on barrier transparency Γ value.

In Fig. 12 we show the behavior of the total Q factor as a function of the barrier. In the extreme quantum regime, compared with Fig. 11, the values of Q^{QIC} and Q for the TUR-R are similar in the case without barrier, $\Gamma = 1$, i.e., the main contribution is due to quantum interference correction. However, for most transparency barrier values Γ, the quantum interference correction for the TUR is negligible compared with its respective total value, indicating that the quantum

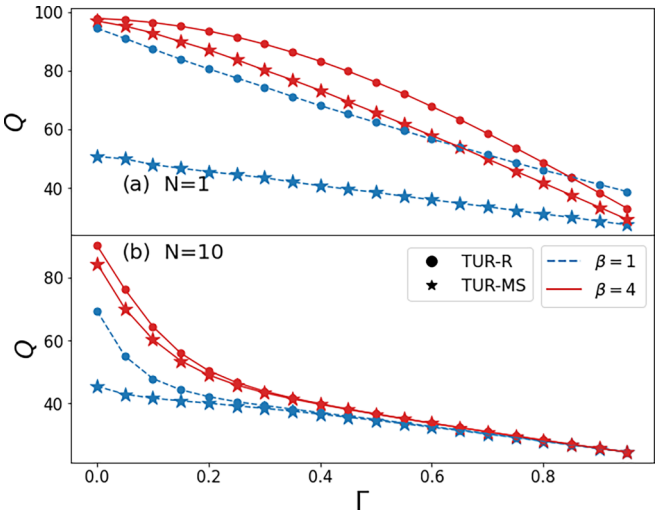

FIG. 12. TUR-R and TUR-MS calculated for the Fano factor values of the ChOrthogonal and ChSymplectic chiral symmetry classes. We perform $\mu = 0.05$ V and $\beta \equiv 1/k_B T \sim 2000$ eV^{-1}. Notice for all values of N and Γ, the quantity Q exhibits values greater than 2 for both TURs. Therefore it can be inferred, based on Eq. (19), that none of the studied chiral CQDs violate the TUR.

interference contribution in chiral quantum dots becomes nonpreponderant. The TUR-R strongly diverges from the ratio between the shot-noise and conductance averages for both Q^{QIC} and Q factor. In the semiclassical regime, we observe that $Q_{\mathrm{TUR-R}} \approx Q_{\mathrm{TUR-MS}}$ for the most transparent barrier values Γ. Finally, since $Q_{\mathrm{TUR-R}} \approx Q_{\mathrm{TUR-MS}}$ in the semiclassical regime, we remark on the validity of the central limit theorem for specific intervals of Γ, which can be observed in Fig. 12.

VI. CONCLUSION

We have investigated the thermodynamic uncertainty relations in mesoscopic systems for all Wigner-Dyson (Schrödinger) and chiral (Dirac) universal symmetry classes: orthogonal, unitary, and symplectic. Based on the random-matrix theory, our analysis starts from the crucial observation that the measure $Q_{\mathrm{TUR\text{-}R}} = \frac{V}{k_B T}[\frac{\langle \mathcal{P} \rangle}{\langle G \rangle}]$ is an intrinsic property of chaotic quantum dots. In this sense it is a novel observable as conductance and the shot-noise power. Furthermore, we demonstrated that the $Q_{\mathrm{TUR\text{-}R}}$ quantity provides a natural way to quantitatively assess the quantum interference effect associated with quantum precision.

Our results clarified the essential role of quantum interference corrections in both categories of Q observable associated with TUR, which we denominate here as TUR-MS, $[\langle \mathcal{P} \rangle]/[\langle G \rangle]$, and the TUR-R, $[\langle \mathcal{P} \rangle / \langle G \rangle]$. The results were obtained for different numbers of open channels and tunneling rates that ranged from the opaque regime (tunneling rate going to zero) to the ideal regime (transparent barrier). Even though the two Q factors tend to be equal in a semiclassical regime due to the central limit theorem (CLT) and the law of large numbers, they are generally different. Thus we analyzed the quantum interference corrections of TUR-R and TUR-MS to establish a connection with the known results of quantum interference corrections for conductance and shot-noise power. Surprisingly, the opaque regime engenders remarkable differences between the Q factors, even in the semiclassical regime, which characterizes a clear violation of the CLT. In particular, the violation of the CLT in the opaque regime suggests that the eigenvalues of Q are not identically distributed for the same spectral regime, characterizing a peculiar nonlinearity of the Q factor in the universal regime.

We also show that the phenomenology associated with quantum interference corrections is strikingly robust for the Q factors, surprisingly being an order of magnitude greater than the supposedly leading semiclassical term. The results of the mesoscopic regime were compared with recent experimental data from electron scattering produced by tunneling junctions. Atomic-scale Au junctions typically generate scattering in the semiclassical regime. Fortuitously, we show that QIC corrections are responsible for an order of magnitude greater results for universal classes when compared to tunneling junctions.

As a consequence, we notice that the TUR-R appears as a novel quantity, which would reveal the discrepancy between the WD quantum-dots simulation and tunneling junction experiment, both in the metallic regime, due to the emergence of the quantum interference phenomenon. Graphene quantum dots and topological insulators have a phenomenology utterly different from the usual metallic regime. Here we describe a way to detect the chirality signal with a very high amplification margin in graphene CQD billiards. Our results open the way for further investigations of heat engines operating in the universal regime with much higher intensity and for studies involving graphene, superconductivity, and other eminently quantum phenomena.

ACKNOWLEDGMENTS

This work was supported by CAPES (Coordenação de Aperfeiçoamento de Pessoal de Nível Superior) and CNPq (Conselho Nacional de Desenvolvimento Científico e Tecnológico).

[1] A. C. Barato and U. Seifert, Phys. Rev. Lett. **114**, 158101 (2015).
[2] P. Pietzonka, F. Ritort, and U. Seifert, Phys. Rev. E **96**, 012101 (2017).
[3] T. R. Gingrich, J. M. Horowitz, N. Perunov, and J. L. England, Phys. Rev. Lett. **116**, 120601 (2016).
[4] G. Benenti, G. Casati, K. Saito, and R. S. Whitney, Phys. Rep. **694**, 1 (2017).
[5] C. W. J. Beenakker, Rev. Mod. Phys. **69**, 731 (1997).
[6] Y. Alhassid, Rev. Mod. Phys. **72**, 895 (2000).
[7] L. P. Kouwenhoven, D. G. Austing, and S. Tarucha, Rep. Prog. Phys. **64**, 701 (2001).
[8] J. G. G. S. Ramos, D. Bazeia, M. S. Hussein, and C. H. Lewenkopf, Phys. Rev. Lett. **107**, 176807 (2011).
[9] J. G. G. S. Ramos, A. L. R. Barbosa, D. Bazeia *et al.*, Braz. J. Phys. **51**, 263 (2021).

[10] B. Kaestner and V. Kashcheyevs, Rep. Prog. Phys. **78**, 103901 (2015).
[11] K. Brandner, T. Hanazato, and K. Saito, Phys. Rev. Lett. **120**, 090601 (2018).
[12] E. Akkermans and G. Montambaux, *Mesoscopic Physics of Electrons and Photons* (Cambridge University Press, Cambridge, England, 2006).
[13] J. G. G. S. Ramos, A. L. R. Barbosa, and A. M. S. Macêdo, Phys. Rev. B **78**, 235305 (2008).
[14] G. P. Papari and V. M. Fomin, Phys. Rev. B **105**, 144511 (2022).
[15] C. Guédon, H. Valkenier, T. Markussen *et al.*, Nat. Nanotechnol. **7**, 305 (2012).
[16] M. S. M. Barros, A. J. Nascimento Júnior, A. F. Macedo-Junior, J. G. G. S. Ramos, and A. L. R. Barbosa, Phys. Rev. B **88**, 245133 (2013).
[17] M. Schneider and P. W. Brouwer, New J. Phys. **16**, 073015 (2014).
[18] Ya. M. Blanter and M. Büttiker, Phys. Rep. **336**, 1 (2000).
[19] C. Schinabeck, R. Härtle, H. B. Weber, and M. Thoss, Phys. Rev. B **90**, 075409 (2014).
[20] R. Vardimon, M. Klionsky, and O. Tal, Phys. Rev. B **88**, 161404(R) (2013).
[21] M. Josefsson, A. Svilans, A. M. Burke, E. A. Hoffmann, S. Fahlvik, C. Thelander, M. Leijnse, and H. Linke, Nat. Nanotechnol. **13**, 920 (2018).
[22] T. Koyuk and U. Seifert, Phys. Rev. Lett. **125**, 260604 (2020).
[23] H. J. D. Miller, M. H. Mohammady, M. Perarnau-Llobet, and G. Guarnieri, Phys. Rev. Lett. **126**, 210603 (2021).
[24] T. Van Vu and K. Saito, Phys. Rev. Lett. **128**, 140602 (2022).
[25] A. M. Timpanaro, G. Guarnieri, J. Goold, and G. T. Landi, Phys. Rev. Lett. **123**, 090604 (2019).
[26] U. Seifert, Rep. Prog. Phys. **75**, 126001 (2012).
[27] C. Jarzynski, Phys. Rev. Lett. **78**, 2690 (1997).
[28] Y. Hasegawa and T. Van Vu, Phys. Rev. Lett. **123**, 110602 (2019).
[29] N. Yunger Halpern, C. D. White, S. Gopalakrishnan, and G. Refael, Phys. Rev. B **99**, 024203 (2019).
[30] F. Dyson, J. Math. Phys. **3**, 1199 (1962).
[31] A. Altland and M. R. Zirnbauer, Phys. Rev. B **55**, 1142 (1997).
[32] H. Weidenmüller and G. Mitchell, Random matrices and chaos in nuclear physics: Nuclear structure, Rev. Mod. Phys. **81**, 539 (2009).
[33] S. Hikami, A. Larkin, and Y. Nagaoka, Prog. Theor. Phys. **63**, 707 (1980).
[34] S. Datta, *Electronic Transport in Mesoscopic Systems* (Cambridge University Press, Cambridge, England, 1995).
[35] H. M. Friedman, B. K. Agarwalla, O. Shein-Lumbroso, O. Tal, and D. Segal, Phys. Rev. B **101**, 195423 (2020).
[36] B. K. Agarwalla and D. Segal, Phys. Rev. B **98**, 155438 (2018).
[37] R. S. Whitney, Phys. Rev. B **75**, 235404 (2007).
[38] L. Huang, H.-Y. Xu, C. Grebogi, and Y.-C. Lai, Phys. Rep. **753**, 1 (2018).
[39] C. Mahaux and H. A. Weidenmüller, *Shell Model Approach to Nuclear Reactions* (North Holland Publishing Company, Amsterdam, 1969).
[40] S. Gustavsson, R. Leturcq, B. Simovič, R. Schleser, T. Ihn, P. Studerus, K. Ensslin, D. Driscoll, and A. Gossard, Phys. Rev. Lett. **96**, 076605 (2006).
[41] M. Field, C. G. Smith, M. Pepper, D. A. Ritchie, J. E. F. Frost, G. A. C. Jones, and D. G. Hasko, Phys. Rev. Lett. **70**, 1311 (1993).
[42] J. Elzerman, R. Hanson, L. Beveren, B. Witkamp, L. Vandersypen, and L. Kouwenhoven, Nature (London) **430**, 431 (2004).
[43] R. Schleser, E. Ruh, T. Ihn, K. Ensslin, D. Driscoll, and A. Gossard, Appl. Phys. Lett. **85**, 2005 (2004).
[44] L. Vandersypen, J. Elzerman, R. Schouten, L. Beveren, R. Hanson, and L. Kouwenhoven, Appl. Phys. Lett. **85**, 4394 (2004).
[45] M. L. Mehta, *Random Matrices* (Academic Press, New York, 1991).
[46] L. A. Ponomarenko, F. Schedin, M. I. Katsnelson, R. Yang, E. W. Hill, K. S. Novoselov, and A. K. Geim, Science **320**, 356 (2008).
[47] E. V. Shuryak and J. J. M. Verbaarschot, Nucl. Phys. A **560**, 306 (1993); J. Verbaarschot, Phys. Rev. Lett. **72**, 2531 (1994).
[48] M. S. M. Barros, I. R. A. C. Lucena, A. F. M. R. Silva, A. L. R. Barbosa, and J. G. G. S. Ramos, Phys. Rev. B **99**, 195131 (2019).
[49] P. W. Brouwer and C. Beenakker, J. Math. Phys. **37**, 4904 (1996).
[50] G. Verley, M. Esposito, T. Willaert, and C. Van den Broeck, Nat. Commun. **5**, 4721 (2014).